Nanotechnology **19** (2008) 145301 (6pp) doi:10.1088/0957-4484/19/14/145301

Evaporative self-assembly assisted synthesis of polymeric nanoparticles by surface acoustic wave atomization

James R Friend[1,3], **Leslie Y Yeo**[1], **Dian R Arifin**[1] **and Adam Mechler**[2]

[1] Micro/Nanophysics Research Laboratory, Monash University, Clayton, VIC 3800, Australia
[2] School of Chemistry, Monash University, Clayton, VIC 3800, Australia

E-mail: james.friend@eng.monash.edu.au

Received 7 January 2008, in final form 5 February 2008
Published 4 March 2008
Online at stacks.iop.org/Nano/19/145301

Abstract
We demonstrate a straightforward and rapid atomization process driven by surface acoustic waves that is capable of continuously producing spherical monodispersed submicron poly-ε-caprolactone particle aggregates between 150 and 200 nm, each of which are composed of nanoparticles of 5–10 nm in diameter. The size and morphologies of these particle assemblies were determined using dynamic light scattering, atomic force microscopy and transmission electron microscopy. Through scaling theory, we show that the larger particle aggregates are formed due to capillary instabilities amplified by the acoustic forcing whereas the smaller particulates that form the aggregates arise due to a nucleate templating process as a result of rapid spatially inhomogeneous solvent evaporation. Minimization of the free energy associated with the evaporative process yields a critical cluster size for a single nucleus in the order of 10 nm, which roughly corresponds with the dimensions of the sub-50 nm particulates.

M This article features online multimedia enhancements

1. Introduction

Polymeric nanoparticles are critical to a wide range of emerging applications, including *in vivo* drug and gene delivery [1], amplification of DNA hybridization biosensors [2], and immunodiagnostics [3]. The conventional techniques currently employed, which include solvent evaporation/extraction [4], spray drying [5], nanoprecipitation [6], and emulsion photocrosslinking [7], typically require multi-step procedures, the use of a considerable amount of solvent, and often result in a wide distribution of particle sizes. Other non-conventional techniques overcome these problems but have troubling drawbacks, as in high voltages for electrospraying [8], for example. In this work we demonstrate the use of surface acoustic wave (SAW) atomization together with a nonuniform evaporation and nucleation process to give sub-50 nm diameter monodisperse nanoparticles. Atomization is a general term for the formation of droplets of one phase in suspension within another from a relatively large interface between the two phases; perhaps the best-known example of atomized droplets are the oil droplets used by Millikan in his famously controversial study on Avogadro's constant [9]. SAW atomization is a simple microfluidics technique that can be carried out on a chip-scale microdevice for portable drug delivery applications or scaled up for industrial production. It employs technology originally developed for the entirely different purpose of signal filtering and multiplexing [10], and provides direct control over the size of the particles by defining the operating frequency of the ultrasonic vibration through the electrode design [11, 12]. Compared to standard ultrasonic atomization techniques [13], it offers far higher operating frequencies and therefore smaller droplet output, and represents a step in the emergence of microfluidics technology in the formation of nanoparticles for targeted drug delivery and other applications [14].

2. Surface acoustic wave atomization

Here the SAW atomization device is a single interdigital transducer (IDT) consisting of 25 pairs of straight electrodes formed of 250 nm aluminum atop a 4 nm titanium layer in

[3] Author to whom any correspondence should be addressed.

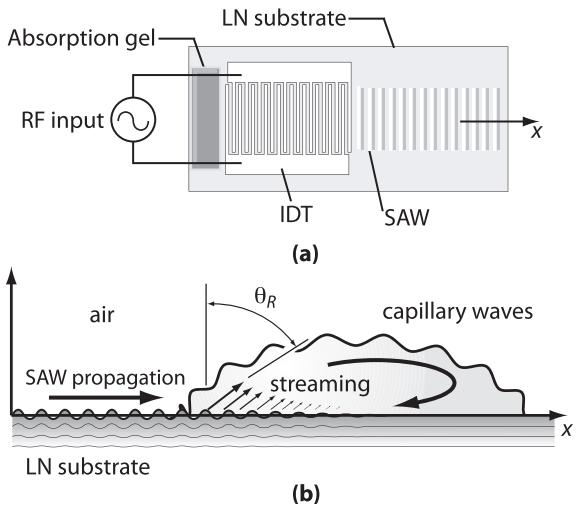

Figure 1. Surface acoustic waves are (a) generated across the LN substrate via an sinusoidal electrical input into the interdigital electrode. Acoustic streaming and subharmonic capillary wave generation [15] (b) occurs in a fluid droplet placed on the substrate as a consequence of interaction with the SAW. The acoustic streaming induces internal recirculation while the oscillatory acoustic field induces the capillary waves.

a basic full-width interleave configuration, sputter-deposited onto a 127.68° *Y*–*X*-cut lithium niobate ($LiNbO_3$ or LN, Roditi UK, Ltd, London) single crystal piezoelectric substrate, as schematically depicted in figure 1(a). Absorption gel (α-gel, Geltec Ltd, Yokohama, Japan) was used to suppress the leftward SAW from the IDT. The SAW wavelength λ was chosen to be 440 μm, thus specifying the operating resonance frequency, 8.611 MHz, and electrode and inter-electrode gaps along the *x*-axis at 110 μm. The IDT finger width perpendicular to the *x*-axis is 10 mm with a gap of 1 mm between the electrode ends and opposite bus bar, which has a width of 3 mm. Application of an oscillating electric field matching the resonance frequency at a power of 300 mW then induces a shallow (3–4λ deep) electroelastic Rayleigh wave [10] along the substrate surface with a displacement of approximately 10 nm, as illustrated in figure 1(b).

Using a syringe pump at a flow rate of 24 ml h^{-1}, we maintained a 25 $\mu\ell$ droplet of the working fluid on the substrate in the path of the SAW, composed of 1% w/w poly-ε-caprolactone (PCL, Sigma-Aldrich Pty. Ltd, Australia) dissolved in acetone; PCL is a biocompatible and biodegradable polymer which is commonly used for *in vivo* controlled release drug delivery [16] due to its combined permeability and slow *in vivo* degradation characteristics into harmless metabolites in 18–24 months, and is indeed promising for uses in other geometries [17]. Transmission of acoustic energy into the liquid drop then occurs through leaky SAW, shown in figure 1(b), which is the diffraction of the axially-polarized compressional wave component of the SAW into the fluid at the Rayleigh angle, θ_R, defined by the ratio of the bulk wave speeds in the substrate and the fluid; for $LiNbO_3$ and water, the Rayleigh angle is $\theta_R = 23°$ [12]. The radiation may be used to move [18, 19], mix [20], or atomize the fluid droplet. As the leaky SAW propagates in the fluid, capillary waves are induced at the liquid–air interface due to excitation of lower-order vibration modes at the liquid interfacial membrane. With sufficient power input into the drop such that the acoustic stress overwhelms the capillary stress, destabilization of the interface occurs resulting in atomization of the liquid, thus producing a fine continuous mist of droplets as shown in the movie (available at stacks.iop.org/Nano/19/145301). As the droplets are ejected, the residual solvent in which the PCL is dissolved evaporates in-flight, leaving behind solid polymer particles. Here, the atomization is carried out at room temperature and 50% relative humidity. For PCL concentrations greater than 1% w/w, a polymer film forms along the substrate surface within a few minutes of operation, reducing the amount of acoustic energy that is allowed to propagate into the drop and therefore reducing atomization efficiency. To maximize the potential yield of the atomization device, we have chosen the maximum feasible concentration of PCL in acetone at 1% w/w for this study.

The PCL solution was first atomized into 50 ml of continuously stirred mixtures of deionized water and surfactant for 20 min placed at varying distances from the SAW device. The surfactants used were sodium dodecyl sulfate (SDS) and Tween-20 (both Sigma-Aldrich Pty. Ltd, Australia); SDS is a common anionic surfactant and Tween-20 is a non-foaming, non-ionic, biocompatible surfactant. The critical micelle concentrations (CMC) of SDS and Tween-20 are 8.7 and 0.06 mM, respectively. Due to the hydrophobic nature of PCL in the surfactant/water mixture, the particles tended to accumulate at the liquid surface, forming large polymer agglomerates. After removing the aggregates from the surface, the suspension was centrifuged at 7000 rpm for 10 min. The aliquot was separated for particle sizing.

3. Particle size measurements

The *z*-average diameter [21] of the suspended particles was measured using a dynamic light scattering (DLS) device (Zetasizer Nano S, Malvern Instruments Ltd, UK), capable of measuring particle sizes in the range 0.6 nm–6 μm for millions to billions of particles. For each set of system parameters, the atomization procedure and particle size measurement was carried out three times.

The particle sizing results from DLS were confirmed using transmission electron microscopy (TEM) and atomic force microscopy (AFM). In the former, PCL nanoparticles were collected into an agitated 0.1% v/v Tween-20 solution, placed 8 cm below the SAW device, and samples of the solution were placed on a TEM substrate (holey support film, 200 mesh copper grid, ProSciTech, Australia) and subsequently air dried in a covered container. The particles were then imaged using a TEM (Phillips CM20, Royal Phillips Electronics, Australia) with a resolution of 0.27 nm. In the latter, 20 $\mu\ell$ of a water/ethanol mixture in which the surfactant-free PCL particles were collected within was pipetted onto atomically flat mica and dried under a nitrogen gas flow for 15 min; the addition of ethanol served to prevent rolling of the particles by the AFM tip due to the water acting as a lubricant [22]. The surface morphology was then imaged

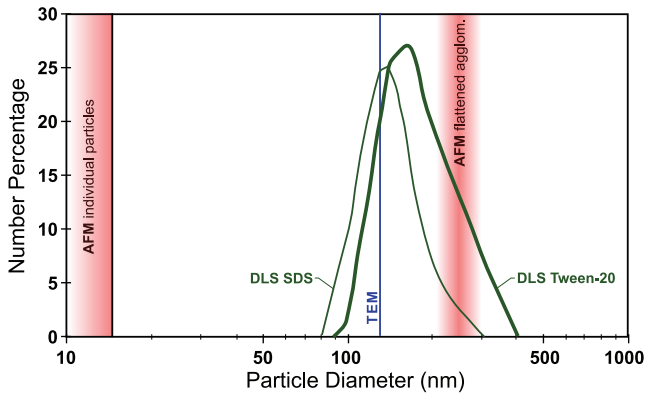

Figure 2. Number percentage size distributions of atomized PCL particles as measured by dynamic light scattering (DLS): DLS SDS is a plot of the DLS results using an 1 mM SDS solution for collection, while DLS Tween-20 is for 0.1%v/v Tween-20. TEM and AFM results are included for comparison.

Table 1. The z-average particle diameters [21] as a function of various process parameters.

SDS (mM)	Tween-20 (% v/v)	Distance (cm)	z-average dia. (nm)
1	—	8	162.3 ± 3.0
10	—	8	153.4 ± 4.0
40	—	8	185.4 ± 4.5
70	—	8	180.2 ± 13.6
100	—	8	177.1 ± 6.9
—	0.1	8	159.8 ± 1.7
—	1	8	169.9 ± 7.6
—	5	8	247.5 ± 3.5
10	—	6	167.3 ± 5.6
10	—	12	214.6 ± 2.5
10	—	16	236.0 ± 61.0
10[a]	—	8	181.4 ± 4.9

[a] The collection solution was sonicated during atomization.

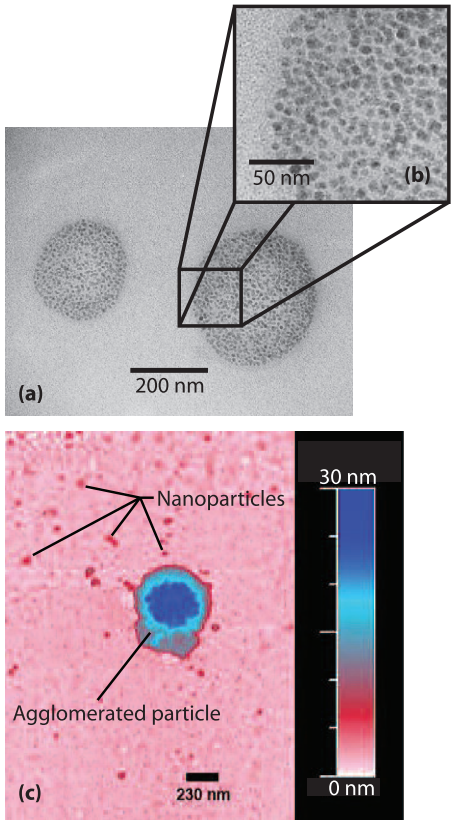

Figure 3. Transmission electron microscopy (TEM) images ((a), (b)) and atomic force microscopy (AFM) images (c) of the particles formed via SAW atomization and solvent evaporation. The particles under closer observation via AFM (c) appear to be agglomerated. Note the flattened morphology of the particle in the AFM—only 30 nm in height—and the appearance of many nanoparticles 5–10 nm in diameter about this agglomeration. Prior to particle deposition the entire atomically flat mica surface would have appeared white in this image.

using a Nanoscope IV Multimode AFM (Veeco, USA) in tapping mode, using MikroMasch NSC15 probes at resonant frequencies of approximately 300 kHz.

The z-average diameters of the nanoparticles produced by the SAW atomization process and collected in SDS and Tween-20 across varying distances from the SAW device, obtained through the DLS measurements, are tabulated in table 1. The smallest particles were obtained for 10 mM SDS and 0.1 % v/v Tween-20 with z-diameters less than 160 nm, though the concentration of either surfactant had little effect on the z-average particle diameter until the concentration was increased well beyond the critical micelle concentration for each surfactant, at which time the average particle diameter increased dramatically. Curiously, as the distance from atomizer to collection fluid is increased from 6 to 8 cm—while holding the other parameters constant—the z-diameter decreases slightly and subsequently *increases* significantly as the separation distance is further increased from 8 to 16 cm. Beyond 16 cm to as much as 50 cm separation distance, the particle diameter remains unchanged. The size distributions of the nanoparticles collected in the lowest SDS and Tween-20 concentrations are shown in figure 2, indicating the particle distributions are both symmetric and monodisperse with either measurement technique. Further, these nanoparticles are noticeably smaller than those generated by a 1.85/5.32 MHz piston atomizer and collected in SDS solutions of similar concentrations [23]. The observed trends also agree with those in Lee *et al* [24], who noted that the particle size increased with the Tween-20 concentration. However, while we expected to improve the monodispersity of the suspensions by sonicating the collection solution during atomization, we note the opposite result from table 1, probably due to agglomeration breakup as discussed later.

TEM images of the nanoparticles are shown in figure 3(a). The average diameter over 21 nanoparticles observed in images like figure 3(a) was 131 ± 32 nm. In addition, the particles were observed to be composed of agglomerations of particles of far smaller diameter, as may be seen in the enlargement figure 3(b); though the morphology of the agglomeration cannot be discerned here using the TEM, the sizes are consistent with the AFM images in figure 3(c), which shows the surface of an atomically flat mica surface covered with spherical nanoparticles with diameters of 5–10 nm. A

larger particle roughly corresponding to the 150 nm order diameters from the DLS measurements and TEM imaging, although flattened either by surface forces or by loss of solvent, may also be observed in figure 3(c). Closer inspection of the surface morphology of this larger particle reveals that it consists of an agglomeration of smaller nanoparticles of similar size to those lying adjacent to the particle agglomerate. Those smaller nanoparticles presumably appear from breakup of the agglomerates while they reside in the collection fluid and during the evaporation of the carrier fluid on the mica substrate. Other 150–200 nm diameter particles similar to those shown (a) are consistently observed in other TEM scans (not shown). The diameter of the 5–10 nm small nanoparticles is neither affected by the distance between the atomizer and the collection fluid, the choice of surfactant, or the concentration of the surfactant, giving some indication of the mechanism of their formation discussed below.

4. Physical process of nanoparticle formation via SAW atomization

The formation of 150–200 nm order agglomerates of 5–10 nm particles can be explained via a twofold process as depicted in figure 4, akin to the self-assembly of silica nanoparticles described by Lu *et al* [25]. Atomization forms microdroplets, figure 4(a), via the Rayleigh mechanism in which the oscillation at the interface due to the presence of the leaky SAW acoustic field in the drop overwhelms the capillary stress at the interface. Destabilization of the interface causes its break up to form a fine mist of atomized droplets. The mean droplet diameter was originally estimated from a balance between the capillary and acoustic stresses by Rayleigh in 1883:

$$D \sim \left(\frac{8\pi\gamma}{\rho f^2}\right)^{1/3}, \qquad (1)$$

where γ and ρ are the surface tension and the density of the liquid, respectively, and f is the frequency of the acoustic radiation. Although the relationship above was first proposed for the case of bulk ultrasonic vibration [11], we note that this scaling holds for any generic process in which the dominant forces are the acoustic and capillary stresses. Lang found empirically that a value of 0.34 was appropriate to include on the right of equation (1) [11], and some have suggested this actually is $1/\pi$ [26], but here we ignore the value because we are looking for an order of magnitude estimate. The factor of eight within the square root, on the other hand, appears due to the subharmonic excitation of the capillary wave, perhaps best modeled by a Mathieu equation [15]. Assuming that the interfacial tension and density of the working fluid is close to that of pure acetone at 25 °C, i.e., 23.7 mN m^{-1} and 0.785 g ml^{-1}, respectively [27, 28], the size of the ejected droplet due to acoustically driven interfacial destabilization is roughly 1 μm.

We assume that complete evaporation of acetone occurs during the fraction of time that the particles are in-flight as illustrated in figures 4(b)–(d), reasonable given the simple diffusion-based prediction of the evaporation of a microdroplet of acetone would occur in microseconds and the time of flight is on the order of a second. We note from the DLS measurements in table 1 that the particle size *increases* with the distance the particle travels before reaching the collection fluid. However, the particle size does not increase beyond 200 nm as the travel distance is further increased beyond 16 cm, and this suggests the solvent is indeed completely evaporating. The increase in diameter may be due to the hardening of the nanoparticle agglomerations before impact at the collection fluid surface: the increase of the mechanical stability of these agglomerates due to the hardening prevents their separation when they 'hit' the surface of the collecting fluid. Assuming that each droplet, on average, contains 1% w/w PCL (density of 1.15 g ml^{-1}), such that the particle volume after complete evaporation of the solvent is roughly 0.68% of the droplet volume, the average particle diameter is between 150 and 200 nm, which is consistent with the DLS and TEM results and the size of the particle agglomerates observed using the AFM.

The appearance of the 5–10 nm particulates that make up the larger particle agglomerates can be explained by a second process that occurs simultaneously during the in-flight evaporation of the solvent. Given that the evaporation occurs at the surface of the ejected droplets, the solute concentration is highest in a thin boundary layer adjacent to the droplet surface. Spatial nonuniformities in the surface evaporative process then result in a thermodynamic instability in which phase separation via spinodal decomposition takes place as a result of the rapid quenching of the temperature. Similar phase separation events are commonly observed in other ejection phenomena.

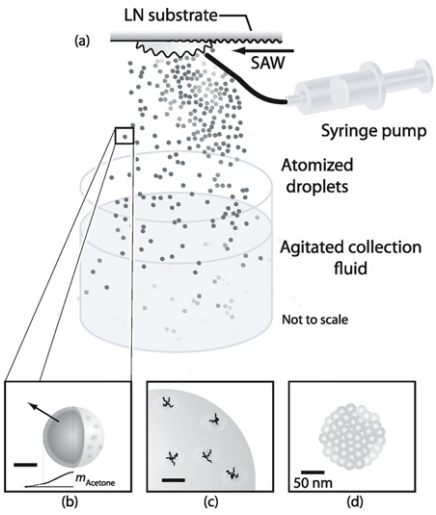

Figure 4. Upon atomization of microdroplets from the lithium niobate substrate via SAW (a), the droplets descend under gravity while (b) the acetone rapidly evaporates from the droplet surface. A nonuniform concentration of acetone, m_{Acetone}, develops within and near the droplet both radially and tangentially along the surface, illustrated by variations in shading in the droplet image. The scale bars are 1 μm in (b) and (c). The droplets are approximately 3 μm in diameter near the atomizer but quickly shrink to around 250 nm as the acetone evaporates. Individual PCL polymer molecules (c) agglomerate upon the droplet surface, providing nucleation sites for subsequent agglomeration (d) to nanoparticle bundles formed for each droplet.

One example is in electrospinning jets, in which the phase separation is responsible for the formation of nanopores on the surface of the fiber [29–31]. In this case, the supercooled-driven phase separation process results in a metastable state in which both solvent-rich and polymer-rich regions exist, as illustrated in figure 4. The latter solidifies much more rapidly than the former thus creating a series of nucleation sites along the surface of the evaporating droplet. The number of these sites is controlled by the solute concentration and solubility.

The above mechanism is corroborated by previous work on PCL-solvent systems [32, 33]. Acetone is known to be a good (hydrophilic) solvent for PCL, having closely matched solubility parameters [33], and tends to promote intra-aggregation between the PCL molecules [32]. Further, a large number of nucleation sites could be expected to form during rapid evaporation [34], and as a result, each nucleation site therefore forms a cluster of PCL molecules until a critical size is achieved. Such template-induced crystalline self-assembly driven by solvent evaporation is well-known in colloidal systems [35].

The critical cluster size can be estimated from classical nucleation theory. Assuming that the properties of each nucleus can be described by bulk properties, the net excess free energy change of a single nucleus with radius R is given by

$$\Delta G_{\mathrm{R}}(R) = \tfrac{4}{3}\pi R^3 \Delta G_{\mathrm{v}} + 4\pi\gamma_{\mathrm{n}} R^2, \tag{2}$$

where ΔG_{v} is the driving force for evaporation and γ_{n} the surface tension of the nucleus. The critical radius R_{c} can then be obtained when ΔG_{R} is a maximum:

$$R_{\mathrm{c}} = \frac{-2\gamma}{\Delta G_{\mathrm{v}}}. \tag{3}$$

Under rapid evaporative-induced supercooled conditions, it is possible to assume that the entropic contribution is small compared to the enthalpy change of vaporization (≈ -540 kJ kg^{-1}). For the polymer concentration used, the critical radius is then estimated to be in the order of 10 nm, commensurate with the 5–10 nm particulates that comprise the larger 150–200 nm order particle aggregates, even though it ignores the subsequent growth of the particles from remaining PCL in the surrounding fluid.

5. Conclusions

To conclude, we have demonstrated a straightforward and rapid technique for the synthesis of spherical monodispersed polymeric nanoparticles through a continuously operating SAW device. At a resonance frequency of 8.611 MHz, submicron particle assemblies between 150 and 200 nm were formed due to acoustically driven atomization via capillary instabilities at the interface of a PCL/solvent drop maintained on the substrate of a SAW device. These large particle aggregates, in turn, are composed of 5–10 nm particles. We attribute these smaller particles to form as a result of a spatially nonuniform solvent evaporation enhanced nucleate templating process. This technique offers a simple approach to efficiently generate very small biocompatible degradeable PCL nanoparticles appropriate for use in drug delivery systems. Its principal promise lies in the flexibility of the method in the use of different solvent–solute systems and the ability to introduce large molecules and other compounds into the atomization fluid for subsequent encapsulation, and this will be the focus of future work in this area.

References

[1] Lu Y and Chen S C 2004 Micro and nano-fabrication of biodegradable polymers for drug delivery *Adv. Drug Deliv. Rev.* **56** 1621–33

[2] Jain K K 2005 Nanotechnology in clinical laboratory diagnostics *Clin. Chim. Acta* **358** 37–54

[3] Wang J 2004 Microchip devices for detecting terrorist weapons *Anal. Chim. Acta* **507** 3–10

[4] Mu L and Feng S S 2002 Vitamin E TPGS used as emulsifier in the solvent evaporation/extraction technique for fabrication of polymeric nanospheres for controlled release of paclitaxel (taxol) *J. Control. Release* **80** 129–44

[5] Hadinoto K, Phanapavudhikul P, Kewu Z and Tan R B H 2006 Novel formulation of large hollow nanoparticles aggregates as potential carriers in inhaled delivery of nanoparticulate drugs *Ind. Eng. Chem. Res.* **45** 3697–706

[6] Craparo E F, Cavallaro G, Bondi M L and Giammona G 2004 Preparation of polymeric nanoparticles by photo-crosslinking of an acryloylated polyaspartamide in w/o microemulsion *Macromol. Chem. Phys.* **205** 1955–64

[7] Zhang G, Niu A, Peng S, Jiang M, Tu Y, Li M and Wu C 2001 Formation of novel polymeric nanoparticles *Acc. Chem. Res.* **34** 249–56

[8] Yeo L Y, Gagnon Z and Chang H C 2005 AC electrospray biomaterials synthesis *Biomaterials* **26** 6122

[9] Millikan R A 1913 On the elementary electrical charge and the Avogadro constant *Phys. Rev.* **2** 109–43

[10] White R M and Voltmer F W 1965 Direct piezoelectric coupling to surface elastic waves *Appl. Phys. Lett.* **7** 314–6

[11] Lang R J 1962 Ultrasonic atomization of liquids *J. Acoust. Soc. Am.* **34** 6

[12] Kurosawa M, Watanabe T, Futami A and Higuchi T 1995 Surface acoustic wave atomizer *Sensors Actuators* A **50** 69–74

[13] Felder C B, Blanco-Príeto M J, Heizmann J, Merkle H P and Gander B 2003 Ultrasonic atomization and subsequent polymer desolvation for peptide and protein microencapsulation into biodegradable polyesters *J. Microencapsul.* **20** 553–67

[14] Gu F X, Karnik R, Wang A Z, Alexis F, Levy-Nissenbaum E, Hong S, Langer R S and Farokhzad O C 2007 Targeted nanoparticles for cancer therapy *NanoToday* **2** 14–21

[15] Benjamin T B and Ursell F 1954 The stability of the plane free surface of a liquid in vertical periodic motion *Proc. R. Soc.* A **225** 505–15

[16] Sinha V R, Bansal K, Kaushik R, Kumria R and Trehan A 2004 Poly-epsilon-caprolactone microspheres and nanospheres: an overview *Int. J. Pharm.* **278** 1–23

[17] Tao S L and Desai T A 2007 Aligned arrays of biodegradable poly(-caprolactone) nanowires and nanofibers by template synthesis *Nano Lett.* **7** 1463–8

[18] Tan W M, Friend J and Yeo L 2007 Microparticle collection and concentration via a miniature surface acoustic wave device *Lab Chip* **7** 618–25

[19] Li H, Friend J R and Yeo L Y 2007 A scaffold cell seeding method driven by surface acoustic waves *Biomaterials* **28** 4098–104

[20] Li H, Friend J and Yeo L 2007 Surface acoustic wave concentration of particle and bioparticle suspensions *Biomed. Microdevices* at press

[21] Bonard J M, Stora T, Salvetat J P, Maier F, Stoeckli T, Duschl C, Forro L, de Heer W A and Chatelain A 1997 Purification and size-selection of carbon nanotubes *Adv. Mater.* **9** 827–31

[22] Murakami H, Kobayashi M, Takeuchi H and Kawashima Y 1999 Preparation of poly (DL-lactide-co-glycolide) nanoparticles by modified spontaneous emulsification solvent diffusion method *Int. J. Pharm.* **187** 143–52

[23] Forde G, Friend J and Williamson T 2006 Straightforward biodegradable nanoparticle generation through megahertz-order ultrasonic atomization *Appl. Phys. Lett.* **89** 064105

[24] Lee Y G, Oh C, Yoo S K, Koo S M and Oh S G 2005 New approach for the control of size and surface characteristics of mesoporous silica particles by using mixed surfactants in W/O emulsion *Micropor. Mesopor. Mater.* **86** 134–44

[25] Lu Y, Fan H, Stump A, Ward T, Rieker T and Brinker C J 1999 Aerosol-assisted self-assembly of mesostructured spherical nanoparticles *Nature* **398** 223–6

[26] Barreras F, Amaveda H and Lozano A 2002 Transient high-frequency ultrasonic water atomization *Exp. Fluids* **33** 405–13

[27] Wohlfarth Ch and Wohlfarth B 1997 *Pure Liquids: Data* (*Landolt-Börnstein* Group IV, vol 16) (Berlin: Springer) (Physical Chemistry: Surface Tension of Pure Liquids and Binary Liquid Mixtures) pp 1–435

[28] Wohlfarth Ch and Wohlfahrt B 2001 *Mixtures of Organic Compounds. Part 3* (*Landolt-Börnstein* Group IV, vol 18A) (Berlin: Springer) (Physical Chemistry: Viscosity of Pure Organic Liquids and Binary Liquid Mixtures, Pure Organometallic and Organononmetallic Liquids, Binary Liquid Mixtures) pp 713–865

[29] Bognitzki M, Czado W, Frese T, Schaper A, Hellwig M, Steinhart M, Greiner A and Wendorff J H 2001 Nanostructured fibers via electrospinning *Adv. Mater.* **13** 70–2

[30] Kim G M, Michler G H and Pötschke P 2005 Deformation processes of ultrahigh porous multiwalled carbon nanotubes/polycarbonate composite fibers prepared by electrospinning *Polymer* **46** 7346–51

[31] Yeo L Y and Friend J R 2006 Electrospinning carbon nanotube polymer composite nanofibers *J. Exp. Nanosci.* **1** 177–209

[32] Tang Z G, Black R A, Curran J M, Hunt J A, Rhodes N P and Williams D F 2004 Surface properties and biocompatibility of solvent-cast poly(-caprolactone) films *Biomaterials* **25** 4741–8

[33] Huang J C, Lin K T and Deanin R D 2006 Three-dimensional solubility parameters of poly(epsilon-caprolactone) *J. Appl. Polym. Sci.* **100** 2002

[34] Leong KH 1987 Morphological control of particles generated from the evaporation of solution droplets: theoretical considerations *J. Aerosol Sci.* **18** 511–24

[35] Hoogenboom J P, Rétif C, de Bres E, van de Boer M, van Langen-Suurling A K, Romijn J and van Blaaderen A 2004 Template-induced growth of close-packed and non-close-packed colloidal crystals during solvent evaporation *Nano Lett.* **4** 205–8